DJS Vol. 45 (1) (2022) pp. 125-140 - ISSN: 1012-5965

Delta Journal of Science

Available online at **https://djs.journals.ekb.eg/**

Research Article **GEOLOGY**

Using a Landsat-8 image for lithological mapping of basement rocks at southeast Aswan city, South Eastern Desert, Egypt

Islam Helal [1], Ibrahim Abu El-Leil [1], Ahmed M. Abdel-Rahman [1], Nehal Soliman [2]

[1] Geology Department, Faculty of Science, Al-Azhar University, PO Box 11884, Nasr City, Cairo, Egypt.
[2] National Authority for Remote Sensing and Space Sciences (NARSS), Cairo 1564, Egypt.

Corresponding author : *Ahmed M. Abdel-Rahman* *e-mail: kady2040@yahoo.com*

KEY WORDS

El-Hudi, lithological mapping, gneiss, migmatite, Landsat-8.

ABSTRACT

The metamorphic rock units and the magmatic rock units constitute their two primary assemblages at southeast Aswan area. The metamorphic assemblage consists of migmatites, gneisses, and hornblende schist. The magmatic rocks comprise two categories: monzogranite and garnetiferous muscovite monzogranite. Schist, migmatite, and gneiss are great examples of rocks that have folded. Granitic rocks invade the metamorphic rock assemblages before being covered by Nubian Sandstones. According to the Landsat-8 results, the FCC RGB-654 and RGB-765, plus band ratio images (3/5, 3/1, 5/7), (7/5, 5/4, 3 /1), (6/2, 6/7, 6/5 * 4/5), PCA-RGB-321, PCA-RGB-421, and PCA-RGB-721 bands are the good results to separate the rock types in this region. The maximum likelihood results for Landsat-8 data show well lithological discrimination between the rock units with the total accuracy 98.26% and Kappa Coefficient 0.9741.

Introduction

Several studies have demonstrated the value of remote sensing in the investigation of mineral deposits, particularly in lithological mapping and the determination of related hydrothermal mineralization in the Egyptian Nubian Shield (e.g., Abu El-Leil, *et al*., 2019; El-Ghrabawy *et al*., 2019; Zoheir, *et al*., 2019; Aboelkhair *et al*., 2021; Khedr *et al*., 2022). The lithological contacts in the present work are most typically identified using multispectral sources of information, such as the Landsat-8 Operational Land Imager (OLI) and Thermal Infrared Sensor (TIRS) data. The study area forms a part of the Neoproterozoic evolution of the Nubian Shield in NE Africa as a result of accretion of inter-oceanic island arc, continental microplates and oceanic plateaus in the course of consolidation of Gondwana (Stern 1994, Abdelsalam and stern, 1996). Three major orogens, the East African Orogen (EAO), the Sahara and Congo-Tanzania cratons to the west, and the Azania and Afif terrains to the east, which together make up one or more continental blocks between the Indian shield and Congo-Tanzania-Bongweula Craton, having shaped the final configuration of greater Gondwana. (Collins and Pisarevisky, 2005).

Study area and Geologic Setting

El-Hudi area is approximately located between latitudes 24º 00′ and 24º 07′ N and longitudes 33º 00′and 33º 16′ E, it is situated about 30 km east of Aswan City and covers around 351 km^2. (Fig.1). The present area is composed of Precambrian rocks covering by Nubian sandstone Formation (Attia, 1995; Hilmy *et al*., 1979; Ragab and El-Gharabawi, 1989; Shaw and Jamesan, 1993; Moghazi *et al*., 2001; Madani and Emam 2009; El-Kazzaz, 2011; Youssef and El-Khodary, 2013; Salem and El Gammal, 2013). According to field geological investigation and given geological map, the studied rock units are represented by gneisses, hornblende schist, monzogranite, garnetiferous muscovite monzogranite, pegmatite, dykes, and veins of Precambrian age (Fig. 2). In the northern and eastern portions of the mapped region, the basement outcrops are unconformably covered by the Nubian sandstones, and they also show up as residual caps in the middle. El-Hudi region is affected by medium to high grade metamorphic rocks intruded by granitic rocks and consider crucial to understanding how folds and thrust faults have developed, (El-Kazza, 2011).

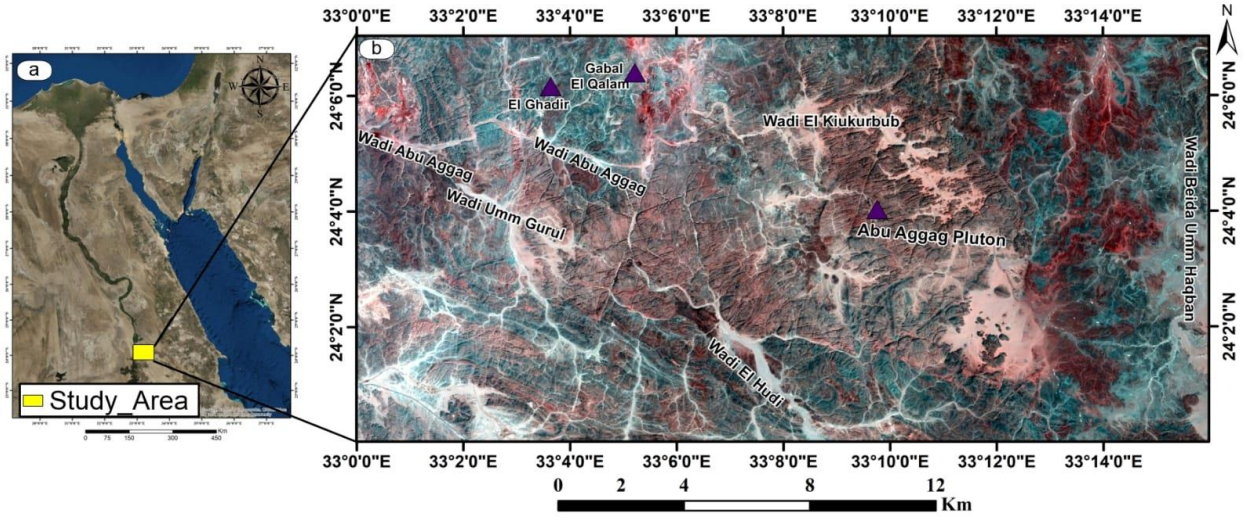

Fig. (1): Location map of the study area, Southeastern part of Aswan area, Egypt.

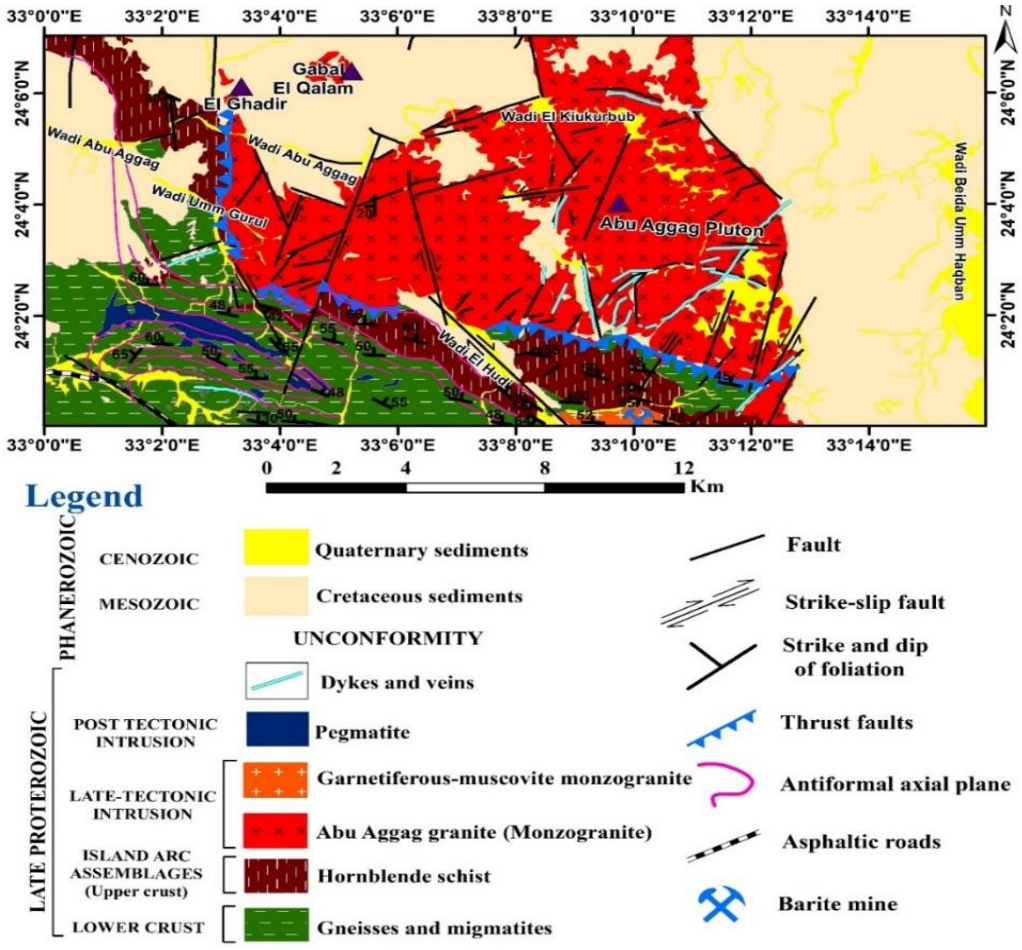

Fig. (2): Geological map of east Aswan area modified after (Emam *et al*., 2011).

Materials and methods

Remote sensing data

The materials and data utilized in this study were gathered from various sources. In this investigation, rock types will be differentiated using Landsat-8 (OLI) data around Wadi El-Hudi area and confirmed by field and microscopic studies. This data covering the study area was acquired separately on September 9, 2020 and downloaded from https://earthexplorer.usgs.gov/.

Landsat-8 was is georeferenced to UTM (Universal Transverse Mercator) and situated in Zone N36 according to WGS-84 datum. The Landsat-8 data used for the study area were digitally processed through ENVI-V.5.1 Software. The pre-processing of remote sensing data using widespread programs (Envi 5.1, Arc GIS 10.3).

The Landsat-8 used a nine-band push-broom sensor to capture data (eight bands at 30 m and one panchromatic band at 15 m ground pixel size), whereas the TIRS used two long-wavelength thermal infrared bands to collect data with a spatial resolution of 100 m. The processed Landsat-8 images will be used for mapping the igneous and metamorphic rocks, which cover the study area. The lithological discrimination and geological mapping of the various basement complex included different processing techniques, e.g., False color Composite images (FCC), band ratio images (Abrams *et al*., 1983, Sultan *et al*., 1986) and principal component analysis (PCA). As well as using two types of supervised classification: Maximum likelihood (ML) and Support vector machine (SVM).

Field investigations

To check how accurate remotely mapped lithologies are the mapped lithological units in El-Hudi area were examined and validated during the field investigation, and rock samples from the different rocks, including metamorphic rocks (migmatite, gneiss, and schist) and intrusive rocks (granite and pegmatite), were gathered. Following the field investigation, spectral reflectance measurements and microscopic analyses were carried out on the obtained rock samples.

Results and discussion

Color composite images

The visual interpretation of color composite images depends on the statistical approach's choice of a better colour composite. The variance within bands and the correlation coefficient between bands are taken into account using the Optimum Index Factor (OIF) techniq (Benomar and Fuling, 2005) and https://doi.org/10.1016/j.oregeorev.2022.105184. The visual inspection of the

highest band-triplet ranks resulted from optimum index factor methods, which yielded that false color composite images RGB-654 and RGB-765 (Figs.3A&B) are the best for lithological differentiation. The false-color composite images RGB-654 and RGB-765 that were employed as an addition to the geological mapping in the current study help to clarify the boundaries between both the structural features and geological units. Figs. (3a and b) are the most successful in discriminating Cretaceous sediments from Abu Aggag monzogranite rocks as well as the folds and faults concentrated in the southern part of area.

Band ratio

Six major color ratio composites have been used to discriminate rock units in the study area, which were evaluated and determined to be the best composites for distinguishing and defining along with lithological contacts. The first band ratio was used by (Sabins *et al*., 1999) (3/5, 3/1, 5/7) for RGB which provides very effective in lithological discrimination showing clear and obvious contacts for the main rock units (Fig.4A). According to Sabins Landsat -8 ratio (3/5, 3/1, 5/7), the Abu Aggag monzogranite and garnetiferous muscovite monzogranite appears in a green-reddish color while the pegmatite and hornblende schist appear in red color. While the second ratio (7/5, 5/4, 3/1) used by (Gad *et al*., 2006) is showing pale green which represented the Abu Aggag monzogranite, the orange color represented the Cretaceous sediments, while the hornblende schist appears in light green color (Fig. 4B).

Recent band ratios used by (Ali-Bik and Hassan 2022) on Landsat images (6/2, 6/7, and 6/5 * 4/5) show very effective lithological discrimination and major folds as well as the dykes distributed in the study area (Fig. 4C). According to this band, the Aggag monzogranite and garnetiferous muscovite monzogranite appear in a deep red color, while the hornblende schist appears in a red-orange color. The Landsat color ratio composites (Figs.4A, B& C) utilized for mapping the lithological units in the region were highly successful.

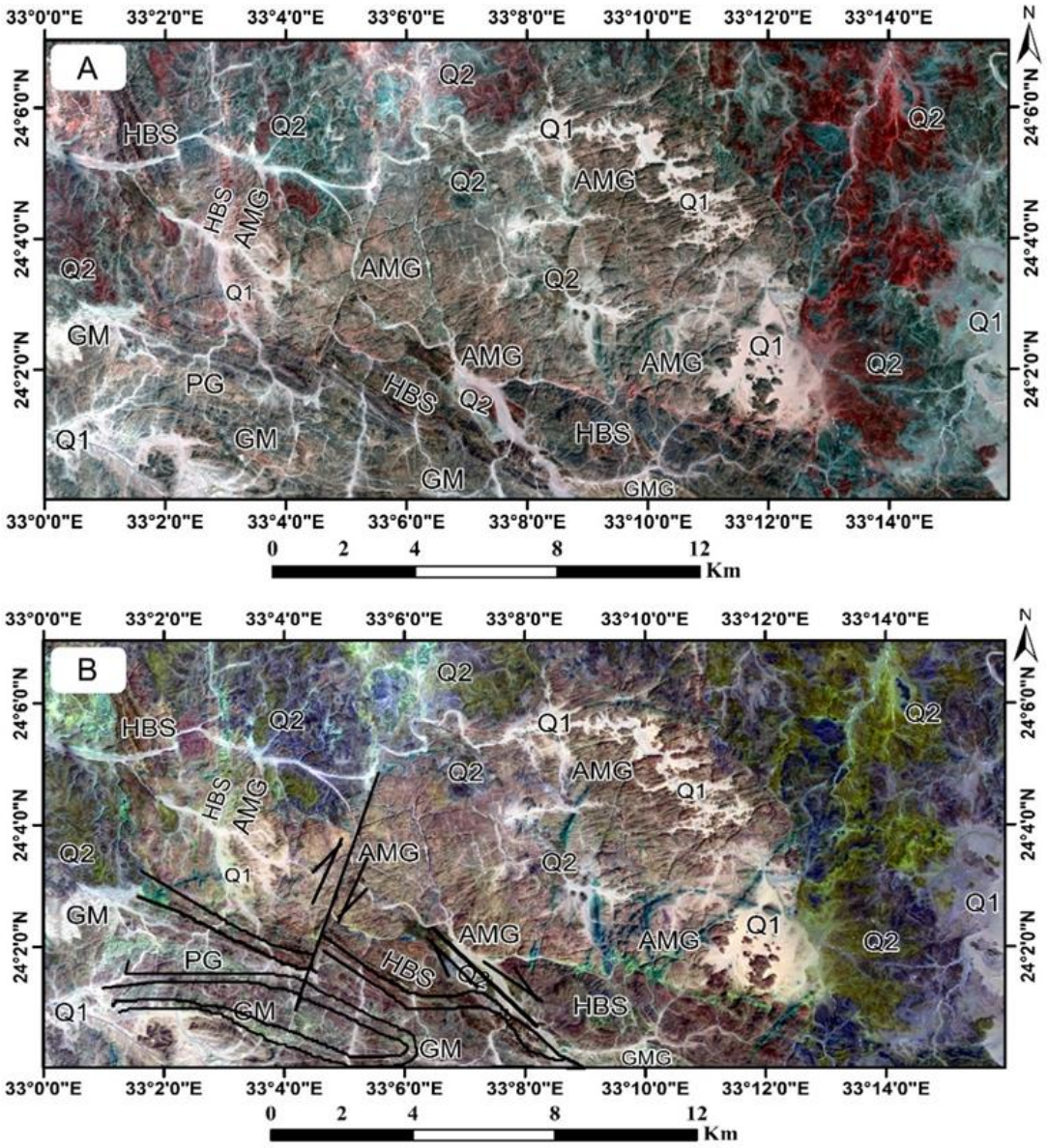

Fig. (3): (A). Landsat-8 color composite image RGB-654 and (B). Landsat-8 color composite image RGB-765. Abbreviation; (Q1) Quaternary sediments, (Q2) Cretaceous sediments, (PG) Pegmatite, (AMG) Abu Aggag Monzogranite, (GMG) Garnetiferous muscovite Monzogranite (HBS) Hornblende schist, and (GM) Gneisses and migmatite.

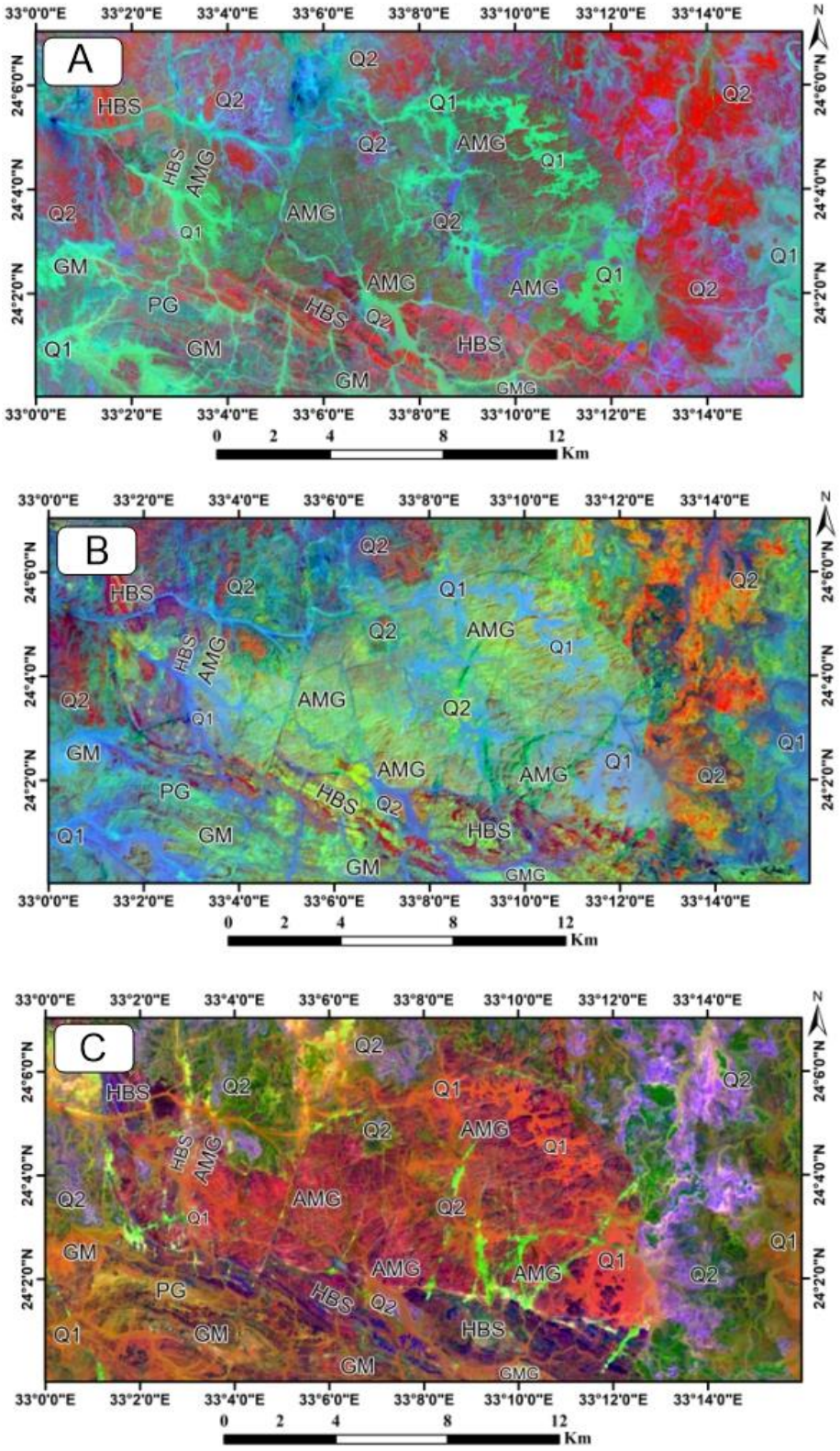

Fig. (4): (A) band ratio of Landsat-8 images (3/5, 3/1, 5/7) in RGB after (Sbins et al., 1999). (B) band ratio of Landsat-8 images (7/5, 5/4, 3/1) RGB after (Gad *et al*., 2006). (C) Band ratio of Landsat-8 images (6/2, 6/7, 6/5 * 4/5) RGB after (Ali-Bik and Hassan, 2022). Symbols as in Fig.3.

Principal component analysis (PCA)

One of the most significant image improvement techniques, principal components analysis (PCA), removes noise components from the original data and decreases their dimensionality (Singh and Harrison, 1985). Through this trend, we can find that false color composite PCA- RGB-321 is represented as the best technique for lithological and structural discrimination with sharp contacts between different rock units.

In this study, the use of the principal component analysis technique resulted in the best three PC combinations of Landsat PCA-RGB-321, PCA- RGB-421, and PCA-RGB 721. These PCs enabled the separation of the different rock units in the study area (Figs. 5A, B& C). PCA-RGB-321, PCA- RGB-421 were used as they have the most informative data with maximum variation and helped in delineating the different rock units and the structure of the study area (Fig. 5C). According to PCA-RGB-321 the Abu Aggag monzogranite rocks exhibit a pale violet color while hornblende schist and Cretaceous sediments rocks are characterized by blue color (Fig. 5A). The dykes are shown in the other PCA bands PCA-RGB-421 as orange, the cretaceous sediments as violet, and the hornblende schist as blue (Fig. 5B). The dykes are the main feature seen in Fig. (5C) according to the final PC bands PCA-RGB-721.

Supervised classification

The image analysis and understanding of the various surface types in the research region play a significant role in the supervised classification process. In the current work, supervised classification was based mainly on spectral signature, with the maximum likelihood (ML) algorithm and depending upon spectral signature by support vector machine (SVM) algorithm to distinguish between different rock units.

Maximum likelihood (ML).

Maximum likelihood classification was widely accepted for lithological mapping using Landsat data by several workers (e.g., Zhang *et al.* 2007 and Fatima *et al*, 2017). Based on field observations, FCC, and band ratio techniques check consideration of the boundary between the rock units in the pre-published geologic map, a representative of each rock unit by Spectral signature file. The geological map was used as a reference to the rock unit boundaries. The present study was applied to the results of maximum likelihood for Landsat-8 data showing

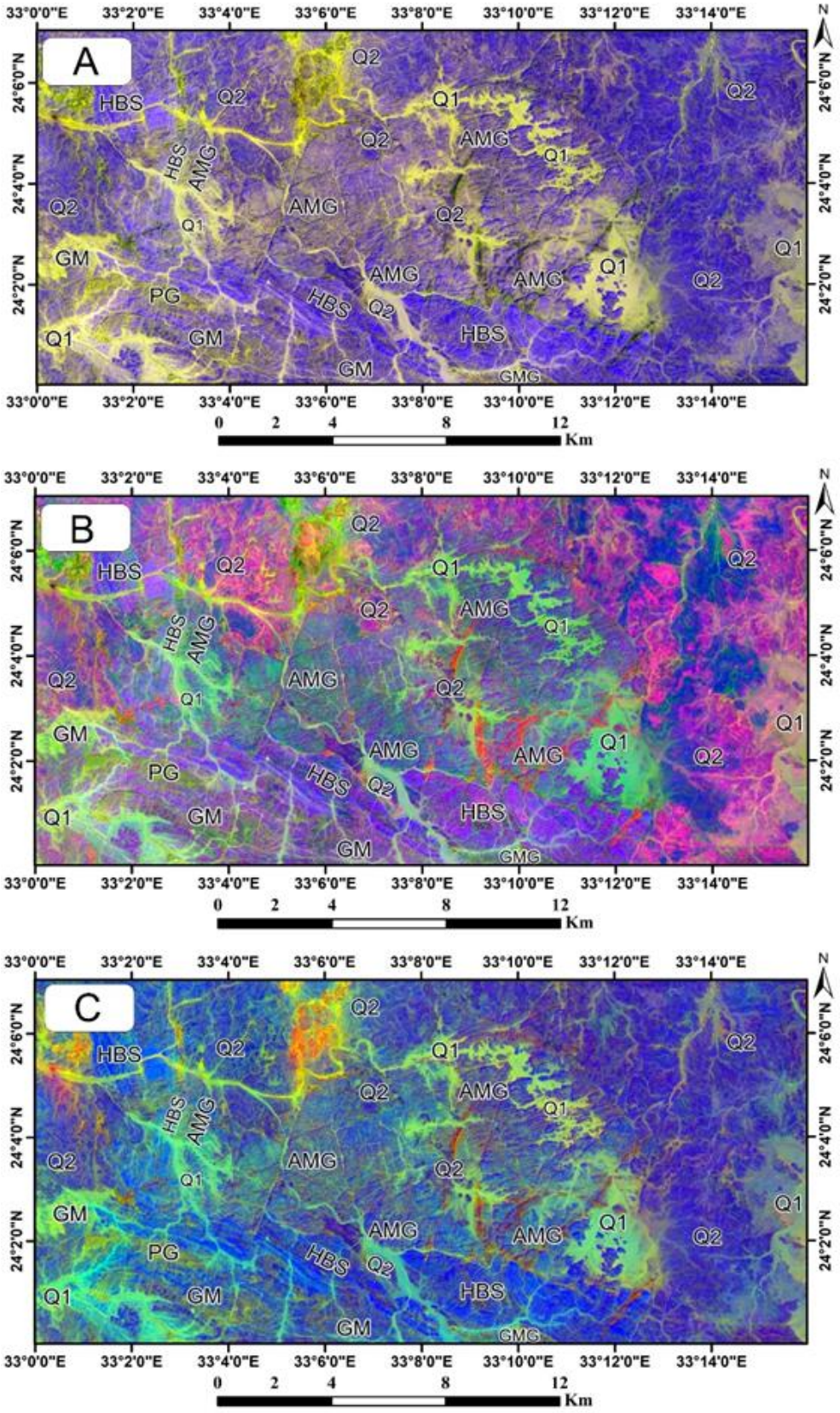

Fig. (5): (A) Landsat-8 PCA image PCA-RGB-321 . (B) Landsat-8 PCA image PCA-RGB-421. (C) PC Landsat-8 PCA image PCA-RGB-721 . Symbols as in Fig.3

well lithological discrimination between the rock units with total accuracy of 98.26% and Kappa Coefficient 0.9741 (Fig. 6A).

Support vector machine.

A classification method called Support Vector Machine (SVM) was suggested with Vapnik, (1999). It is a supervised classification algorithm that was created using a statistical learning methodology and is recommended for dealing with complex class distributions in multi- and hyperspectral image data (Mountrakis, *et al.*, 2011; Liesenberg *et al.*, 2013). In the present study, SVM classification showed well lithological discrimination between the rock units with an overall accuracy of 97.60% and a Kappa coefficient of 0.964. High accuracy and Kappa values indicated the suitability of this classification technique on Landsat-8 data for areas with similar characteristics as that of the study area. In the resulting classification map, the rock units are represented in (Fig. 6B).

Field validation and Petrographic analysis

According to field investigations, the central, eastern, and western regions of the El Hudi area are occupied by the rocks known as gneisses and migmatites, as well as they represent the oldest rock units in the study area. They have well-foliated, banded structures, and exhibit as fine- to medium-grained texture (Fig. 7A). According to petrographic study the investigated gneisses are medium-coarse-grained rocks, usually characterized by well-developed gneissose, augen and porphyroblastic textures. They are composed essentially of quartz, biotite, plagioclase, and K-feldspars (Fig. 7B), while most of the investigated migmatites are formed of successive layers of melanosomes and leucosomes with clears gneissose texture, in addition to augen and porphyroblastic textures (Fig. 7C). The leucosomes are represented by plagioclase and quartz, while the melanosomes are represented by biotite, hornblende, and augite minerals (Fig. 7D).

The hornblende schist occasionally, it occurs as highly schistose rock, highly jointed along the NW trend coinciding with the same direction of the schistosity plane (Fig. 7E). Petrographically, they usually grey and dark green color and subordinate lepidoblastic and poikiloblastic textures. It consists mainly at hornblende, augite, quartz, plagioclase, and biotite in addition to epidote and iron oxides as secondary and accessory minerals (Fig. 7F). The granitic rocks are classified to two types: monzogranite and garnetiferous muscovite monzogranite.

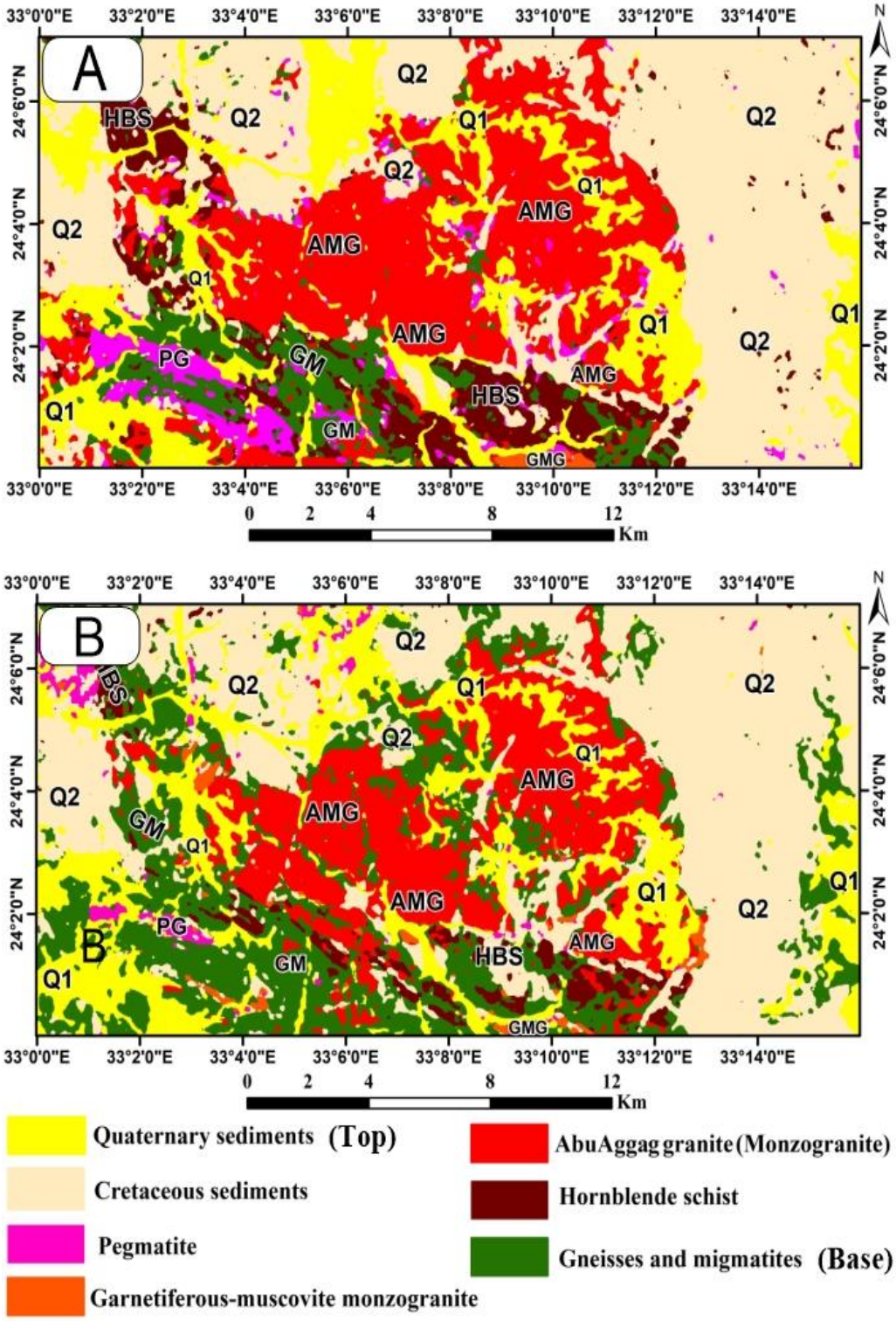

Fig. (6): (A) Maximum Likelihood classification of Landsat-8 bands. (B) Support vector machine classification of Landsat-8 bands.

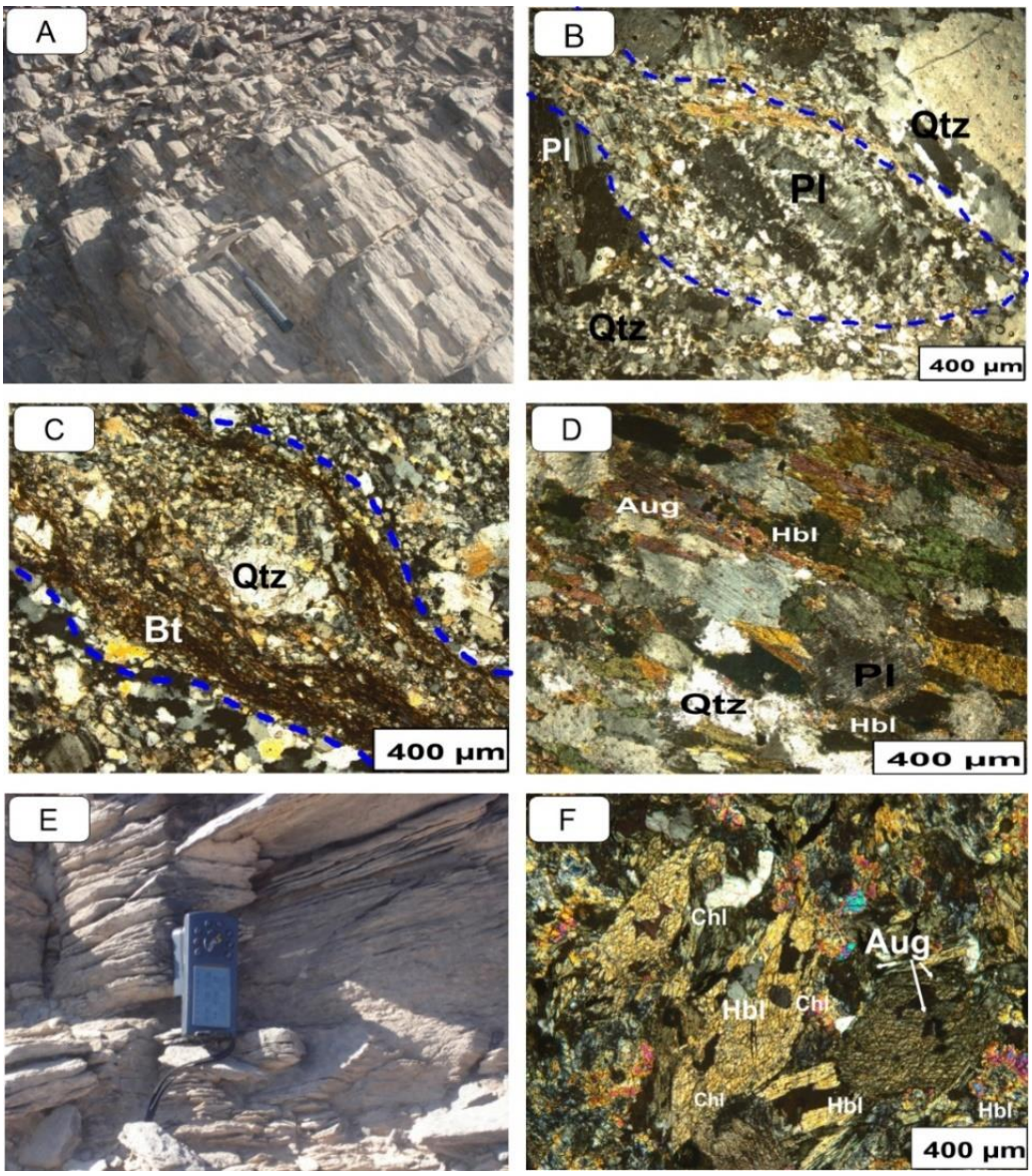

Fig. (7): The plate showing **(A)** highly foliated and jointed gneiss outcrop. **(B)** augen texture and undulose or mylonitized quartz (Qtz) in gneisses. **(C)** augen texture and mylonitization of larger quartz (Qtz) in migmatites. **(D)** melano-bands alternated with leucosome band in the migmatite rocks. **(E)** highly schistose rock in hornblende schists. **(F)** well-developed two sets cleavage crystals of hornblende (Hbl) and showing augite crystals in hornblende schist.

The **monzogranite** is mainly represented by the Abu Aggag granitic pluton, covering a considerable area in the northern part of the mapped area, (Fig. 2). They are often coarse to medium grained texture and buff color. The monzogranite of Abu Aggag pluton is extensively dissected by several strike-

slip and dip-slip faults that have N-S, NNW-SSE, NNE-SSW, ENE-WSW trends, resulting in high shearing, fracturing, and jointing of rocks (Figs. 8A & B). Microscopically, these rocks are characterized by hypidiomorphic perthitic and poikilitic textures, (Figs. 8C&D). It consists mainly of plagioclase, microcline, quartz, biotite and few amount of muscovite.

The **garnetiferous muscovite monzogranite** is represented by a small mass lying nearby wadi El-Hudi at the southern part of the mapped area, (Fig. 2). Petrographically, they exhibit hypidiomorphic and granular textures, consisting mainly of K- feldspars, quartz, plagioclase, muscovite, garnet, and biotite, whereas zircon and iron oxides are the main accessory minerals (Figs. 8E-H).

Conclusions

The study area belongs to the southern part of the Eastern Desert. The studied rock units are represented basement rocks (gneisses, hornblende schist, garnetiferous muscovite monzogranite, monzogranite, pegmatite, dykes, and veins of Precambrian age), unconformably covered by the Nubian sandstone. Gneisses are composed essentially of quartz, biotite, plagioclase, and K-feldspars. Migmatites are formed of successive layers of melanosomes and leucosomes. Hornblende schist is consisting mainly at hornblende, augite, quartz, plagioclase, and biotite in addition to epidote and iron oxides as secondary and accessory minerals. The monzogranite consists mainly of plagioclase, K-feldspars, quartz, biotite and few amount of muscovite. Garnetiferous muscovite monzogranite is consisting mainly of K- feldspars, quartz, plagioclase, muscovite, garnet, and biotite, whereas zircon and iron oxides are the main accessory minerals.

On the other place, FCC, BR, and PCA combined with geological maps could produce a reference lithological map. According to Landsat-8 FCC (6, 5, 4) and (7,6,5), in addition to band ratio images (3/5, 3/1, 5/7), (7/5, 5/4, 3/1) and (6/2, 6/7, 6/5*4/5) and PCA (PC321, PC421, and PC721) distinguished the various lithological units in the region area depending on the properties of their spectral range. Supervised classification was applied depending on regions of interest (ROI), with maximum likelihood (ML) and support vector machine (SVM) by the ability of a different algorithm to distinguish between different rock units.

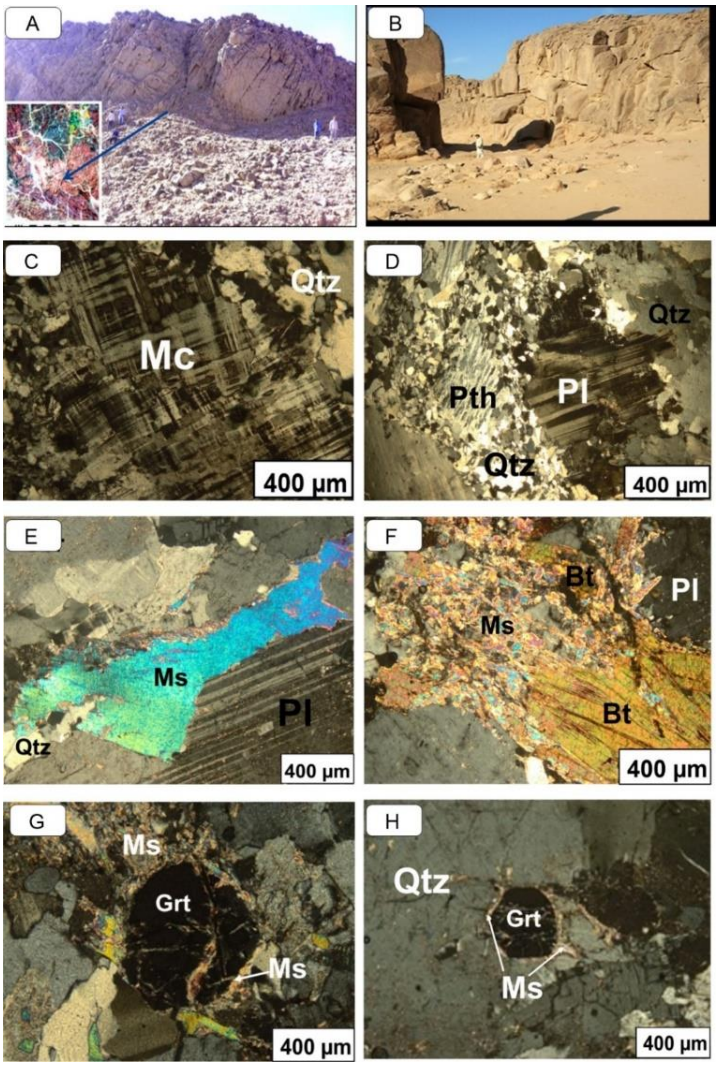

Fig. (8): **(A)** two oblique sets of joints in Abu Aggag granite pluton. **(B)** high masses of Abu-Aggag granite pluton. **(C)** large crystals of tartan microcline (Mc) . **(D)** fine grains of quartz (Qtz) associated plagioclase (Pl) and perthite (Pth) texture**(E)** lamellar twinning plagioclase (Pl) associated with muscovite. **(F)** large muscovitized biotite crystal (Bt) and plagioclase (Pl) to sericite (Ser). **(G)** coarse grain of garnet (Grt) surrounding by muscovite (Ms) and sericite (Ser). **(H)** euhedral to subhedral garnet (Grt) set in a quartz matrix (Qtz).

References

Abdelsalam, M.G. and Stern, R.J., 1996. Sutures and shear zones in the Arabian-nubian shield. *J. Afr. Earth Sci.*, 23:289–310.

Aboelkhair, H., Ibraheem, M., & El-Magd, I. A., 2021. Integration of airborne geophysical and ASTER remotely sensed data for delineation and mapping the potential mineralization zones in Hamash area, South Eastern Desert, Egypt. *Arab. J. Geosci.*, 14(12): 1-22

Abu El-Leil, I., Soliman, N.M.A , Bekiet, M.H. and Elhebiry, M.S., 2019. Enhancing multispectral remote sensing data interpretation for historical gold mines in Egypt: a case study from Madari gold mine. *Arab. J. Geosci.*, 12: 3.

https://doi.org/10.1007/s12517-018-4081-6.

Abrams, M.J., Brown, D., Lepley, L. and Sadowski, R., 1983. Remote sensing for porphyry copper deposits in southern Arizona. *Economic Geol.*, 78:591–604.

Ali-Bik, M., Hassan, S., 2022.Remote sensing-based mapping of the Wadi Sa'al-Wadi Zaghara basement rocks, southern Sinai, Egypt. *Egypt J. Remote Sensing and Space Sci. DOI: 10.1016/j.ejrs.2022.03.015.*

Attia, M.J. and Murray, G.W., 1955. Lower Cretaceous ammonites in marine intercalations in the "Nubian Sandstone" of the Eastern Desert of Egypt, *Quart. J. Geol. Soc. London*, v. 107: 442–443.

Benomar, T. and Fuling, B., 2005. Improved geological mapping using Landsat-5 TM data in Weixi area, Yunnan Province China. *Geo-Spatial Information Sci.,* 8: 110–114.

Collins, A.S. and Pisarevsky, S.A., 2005. Amalgamating Eastern Gondwana: the evolution of the Circum-Indian Orogens. Earth Science Reviews, V. 71, pp. 229–270. Costa, R.D. and Starkey, J., 2001. Photo Lin: a program to identify and analyze linear structures in aerial photographs, satellite images and maps. *Computers & Geosci.*, 27: 527–534.

El-Ghrabawy, O., Soliman, N. and Tarshan, A., 2019. Remote sensing signature analysis of ASTER imagery for geological mapping of Gasus area, central eastern desert Egypt. *Arab. J. Geosci.* 12:408.

El-Kazzaz, Y.A., 2011. Geometry of fold interference patterns in Wadi Kharit area, South Eastern Desert, Egypt. *Egypt J. Remote Sensing and Space Sci.,* 13: 113-120.

Emam, A., Moghazy, N.M. and El-Sherif, A.M., 2011. Geochemistry, petrogenesis and radioactivity of El Hudi I-type younger granites, South Eastern Desert, Egypt. *Arab. J. Geosci.*, 4: 863–878.

Fatima, K., Khattak, M., Kausar, A., Toqeer, M., Haider, N.and Ur Rehman, A., 2017. "Minerals identification and mapping using ASTER satellite image. *J. of Appl., Remote Sensing,* 11(4)*:* P. 046006.

Gad, S., Kusky, T. ,2006. Lithological mapping in the Eastern Desert of Egypt, the Barramiya area, using Landsat thematic mapper (TM). *J. Afr. Earth Sci.,* 44: 196–202.

Hilmy, M., 1979. Petrography and chemistry of the granitic rock and the overlying Nubian Sandstone in Bir Umm Hibal area, Southeast of Aswan, Eastern Desert, Egypt. *Acta Mineralogical petrographica Szeged,* pp. 41-62.

Liesenberg, V. and Gloaguen, R. ,2013. Evaluating SAR polarization modes at L-band for forest classification purposes in Eastern Amazon, Brazil. Int. *J. of Appl. Earth Observation and Geoinformation,* 21:122–135.

Madani, A.A. and Emam, A.A., 2009. SWIR ASTER band ratios for lithological mapping and mineral exploration: A case study from El Hudi area, Southeastern Desert, Egypt. *Arabian J. Geosci.* 4: 45–52.

Moghazi, A.M., Hassanen, M. A., Hashad, M. H. and Mohamed, F. H., 2001. Garnet- bearing leucogranite in the EI-Hudi area, southern Egypt: evidence of crustal anatexis during Pan-African low pressure regional

Khedr, M. Z., Abo Khashaba, S. M., El-Shibiny, N. H., El-Arafy, R. A., metamorphism. *J. Afr. Earth Sci.*, 33(2): 245¬259.

Mountrakis, G., Im, J. and Ogole, C., 2011. Support vector machines in remote sensing: A review. ISPRS *J. Photogramm. Remote Sensing,* 66(3): 247–259.

Ragab, A. I. and El-Gharabawi, R. I., 1989. Wadi El-Hudi migmatites, east of Aswan, Egypt: a geological study and some geotectonic implications for the Eastern Desert of

Egypt. *Precambrian resch.*, 44(1): 67-79.

Sabins, F.F., 1999. Remote sensing for mineral exploration. *Ore. Geo. Rev.* 14: 157–183.

Salem, S.M. El-Gammal, E.A., and Greiling, R.O., 2013. Applications of geomorphology, tectonics, geology, and geophysical interpretation of, East Kom Ombo depression, Egypt, using Landsat images Egypt. *J. Remote Sens. Space Sci.*, 16: 171-187, *10.1016/j.ejrs.2013.05.001*.

Shaw, I. and Jameson, R., 1993. Amethyst mining in the Eastern Desert: a preliminary survey at Wadi el-Hudi. *J. Egy. Arch.*, 79(1): 81-97.

Singh, A., Harrison A., 1985. Standardized Principal Components. *Int. J. Sens.* 6 (6): 883–896.

https://doi.org/10.1080/01431168508948511.

Stern, R.J., 1994. Arc assembly and continental collision in the Neoproterozoic East African Orogen: implications for the consolidation of Gondwanaland. *Annul. Rev. Earth Planet. Sci.*, 22:319–351.

Sultan, M., Arvidson, R.E. and Sturchio, N.C., 1986. Mapping of serpentinites in the Eastern Desert of Egypt using Landsat Thematic Mapper data. *Geol.*, 14: 995–999.

Vapnik, V.N., 1999. The Nature of Statistical Learning Theory, 2nd ed.; Springer: *New York, NY, USA.*

Youssef, M.A.S and Elkhodary, S.T., 2013. Utilization of airborne gamma ray spectrometric data for geological mapping, radioactive mineral exploration and environmental monitoring of southeastern Aswan city, South Eastern Desert, Egypt, Geophys. *J. Int.*, 195.

Zhang, X., Pazner, M. and Duke, N., 2007. Lithologic and mineral information extraction for gold exploration using ASTER data in the south Chocolate Mountains (California). *Photogrammetry and Remote Sensing*, 62(4): 271-282.

Zoheir, B., Emam, A., Abd El-Wahed and M., Soliman, N., 2019a. Gold endowment in the evolution of the Allaqi-Heiani suture, Egypt: a synthesis of geological, structural, and space- borne imagery data. *Ore Geol. Rev.* *https://doi.org/10.1016/j.oregeorev.2019.102938.(46)*.

استخدام صور القمر الصناعي لاند سات ٨ لفصل لتحديد الواحدات الصخرية لصخور القاعدة بمنطقة جنوب شرق أسوان ، جنوب الصحراء الشرقية – مصر

إسلام هلال [١] ، إبراهيم أبوالليل [١] ، أحمد مصطفي عبدالرحمن [١] ، نهال سليمان[٢]

[١] قسم الجيولوجيا ـ كلية العلوم – جامعة الأزهر
[٢] الهيئة القومية للإستشعار عن بعد وعلوم الفضاء ـ القاهرة

يتواجد بمنطقة الدراسة مجموعتين من الصخور المتحولة وهي صخور النيس والميجماتيت وصخور الهورنبلند شيست بالإضافة إلي وحدات الصخور الصهارية التي تتكون من صخور المونزوجرانيت وصخور الجارنت مسكوفيت مونزوجرانيت وهذه الصخور قاطعة صخور النيس والشيست وكل هذه الصخور مغطاه بصخور الفانيروزويك من الحجر الرملي.

وتلخصت نتائج الاستشعار عن بعد أنه تم اختيار أفضل مجموعة نطاقات باستخدام تقنية (OIF) وأن أفضل مجموعة نطاقات بالنسبة لبيانات لاند سات ٨ هي (٦,٥,٤) و(7,5,٦).وتم تطبيق تقنيات التصنيف متعدد الأطياف وتم تطبيق طريقتين في التصنيف المراقب Supervised هما (ML and SVM) للتميز بين الوحدات الصخرية المختلفة من خلال استخدام خوارزميات مختلفة.وتم استخدام تقنية العالقات النسبية المطابقة لنسب أخرى مثل (٥/٧ ، ٤/٥ ، ٣/١) ، و (٧ /٥ ، ١ /٥ ،(٤/٣)* ٤ /٥) .وتم استخدام نطاقات سطوع PC1و PC2 وPC3 بالإضافة إلي نطاقات PC1 و PC2 و PC4 في RGBلبيانات ٨-Landsat.